N69-15308
NASA CR-~~65308~~
99006

# BOUNDARY CORRECTIONS FOR A COAXIAL THREE-COIL CONDUCTIVITY/VELOCITY PLASMA PROBE

by

Vikram K. Kinra

CASE FILE
COPY

# BOUNDARY CORRECTIONS FOR A COAXIAL THREE-COIL CONDUCTIVITY/VELOCITY PLASMA PROBE

by

Vikram K. Kinra

A thesis submitted in partial fulfillment
of the requirements for the degree

of

MASTER OF SCIENCE

in

Mechanical Engineering

Approved:

Major Professor

Head of Department

Dean of Graduate Studies

UTAH STATE UNIVERSITY
Logan, Utah

1968

## ACKNOWLEDGMENTS

I wish to thank Dr. Edward W. Vendell, my major professor, for his immense understanding and patience during the course of this investigation. I extend a deep appreciation and thanks to him for his advice and stimulating discussions in preparation of this thesis.

I would like to thank Dr. Alma P. Moser and Dr. Owen K. Shupe, members of my graduate committee, for a review of this paper.

To the National Aeronautics and Space Administration, who provided the funds for this project, go my thanks and sincere appreciation.

Thanks are also due to Mr. James Jeske of Ames Research Center, Moffett Field, California for allowing me to use his Gaussian quadrature computer program.

To Dr. Edward W. Vendell, once again, and to Professor Alexander R. McKay, do I express my gratitude for the inspiration that I derived from them during the course of my academic activities at Utah State University.

Finally, the work is dedicated to my dear mother, whose incessant love, and to my dear father, whose memories have been a perpetual source of inspiration during my academic career.

Vikram K. Kinra

TABLE OF CONTENTS


| Chapter | | Page |
|---|---|---|
| I. | INTRODUCTION . . | 1 |
| II. | PREVIOUS INVESTIGATIONS . | 4 |
| III. | THEORY OF THE INSTRUMENT . . . . . | 10 |
| | Theory of Rossow and Posch . . . . . | 10 |
| | Modified Probe Theory for a Cylindrically Bounded Medium by Vendell . . . . . | 16 |
| | Analysis of a Three-Coil Coaxial Probe Configuration . . . . . | 22 |
| | Electrical conductivity . . . | 25 |
| | Product of conductivity and and velocity or $\sigma U_{\parallel}$ . . . . . | 28 |
| | Numerical evaluation of boundary correction factors | 31 |
| | Hub correction factors . . . . . | 36 |
| | Calibration Equations for the Coaxial Probe . . . | 40 |
| IV. | COMPARISON OF THEORETICAL AND EXPERIMENTAL RESULTS . . . . . | 45 |
| V. | CONCLUDING REMARKS . . . . . | 56 |

Page

LITERATURE CITED . . . 58

VITA . . . . . 61

## LIST OF TABLES


| Table | | Page |
|---|---|---|
| 1. | Conductivity correction factors $\theta_{\Sigma}$ . . . . . | 35 |
| 2. | Velocity correction factors $\theta_{T}$ . . . . . | 35 |
| 3. | Characteristics of probes tested . . . . . | 46 |
| 4. | Values of electrical conductivity using calibration equation and conductivity cell . . . . . | 50 |
| 5. | Experimental verification of the theoretical values of the conductivity hub correction factors . . . . . | 55 |

## LIST OF FIGURES


| Figure | | Page |
|---|---|---|
| 1. | Schematic sketch of the three-coil coaxial, conductivity velocity plasma probe . . . . | 23 |
| 2. | Schematic sketch showing the position of the probe inside the cylindrical boundary . . . | 23 |
| 3. | Conductivity boundary correction factor $\theta_\Sigma$ as a function of the radial position parameter P for several typical values of the coil spacing parameter $D = d/R$ . . . . . | 32 |
| 4. | Conductivity boundary correction factor $\theta_\Sigma$ as a function of the coil spacing parameter D for several typical values of the radial position parameter $P = \rho/R$ . . . . . | 33 |
| 5. | Velocity boundary correction factor $\theta$ as a function of radial position for the case $D = d/R = 0.30$ . . | 34 |
| 6. | Conductivity and velocity hub correction factors that compensate for the perturbation current loops which cannot exist in the region occupied by the coaxial probe . . . . . | 39 |
| 7. | Center line probe reading $\phi_\Sigma$ as a function of reciprocal of container diameter $(2R)^{-1}$ for probe C . . . . . | 47 |
| 8. | Center line probe reading $\phi_\Sigma$ as a function of reciprocal of container diameter $(2R)^{-1}$ for probe B . . . . . | 48 |
| 9. | Comparison of numerical calculations of $\theta_\Sigma$ with experimental data taken by a coaxial probe in cylinders of salt solution . . . . . | 52 |

Figure | Page

10. Comparison of numerical calculations of $\theta_\Sigma$ with experimental data taken by a coaxial probe in cylinders of salt solution for the case $P = \rho/R = 0.0$ . . . . . 53

## LIST OF SYMBOLS

| | | |
|---|---|---|
| $\overline{A}$ | = | vector potential function |
| $\overline{B}$ | = | magnetic induction vector |
| $\overline{B}_p$ | = | primary dipole magnetic induction vector |
| $\overline{b}_t$, $\overline{b}_{\parallel}$ | = | first-order magnetic induction vectors |
| $\overline{E}$ | = | electric field intensity vector |
| $I_p$ | = | total current, primary coil |
| $\overline{J}$ | = | current density vector |
| $\overline{J}_t$, $\overline{J}_{\parallel}$ | = | first-order current density vectors |
| $n_p$ | = | number of turns, primary coil |
| $n_s$ | = | number of turns, secondary coils |
| $Q_o$ | = | quality factor of an electric circuit |
| $R$ | = | radius of a cylindrical region |
| $R_m$ | = | magnetic Reynolds number |
| $r$ | = | distance in spherical coordinates |
| $r_p$ | = | characteristic radius, primary coil |
| $r_s$ | = | characteristic radius, secondary coils |
| $t$ | = | subscript refers to first-order fields caused by $\sigma$ |
| $\overline{U}$ | = | velocity vector |
| $U_{\parallel}$ | = | axial velocity component |
| $X, Y, Z$ | = | dimensionless Cartesian coordinates |

| | | |
|---|---|---|
| $x, y, z$ | = | Cartesian coordinates |
| $\theta_{\Sigma}$ | = | boundary correction factor for $\sigma$ |
| $\theta_{\Upsilon}$ | = | boundary correction factor for $\sigma U_{\parallel}$ |
| $\mu$ | = | magnetic permeability |
| $\rho$ | = | distance of probe from z-axis along negative x-direction |
| $\sigma$ | = | electrical conductivity |
| $\phi_{\Sigma}$ | = | sum of signals induced on two secondary coils |
| $\phi_{\Sigma\infty}$ | = | sum of signals induced on two secondary coils in an unbounded medium |
| $\phi_{\Upsilon}$ | = | difference of signals induced on two secondary coils |
| $\phi_{\Upsilon\infty}$ | = | difference of signals induced on two secondary coils in an unbounded medium |
| $\omega$ | = | frequency of impressed power |
| $\parallel$ | = | subscript refers to first-order fields caused by $\sigma U_{\parallel}$ |

ABSTRACT

Boundary Corrections for a Coaxial Three-Coil

Conductivity/Velocity Plasma Probe

by

Vikram K. Kinra, Master of Science

Utah State University, 1968

Major Professor: Dr. Edward W. Vendell
Department: Mechanical Engineering

Rossow and Posch have proposed several configurations of immersible three-coil devices that measure local values of electrical conductivity and velocity in unbounded conducting fluids at low magnetic Reynolds numbers. Using a previously tested configuration of three coils mounted on separate support rods, Vendell extended the theory to account for the presence of a finite cylindrical boundary. The present work is concerned with an improved probe that further decreases the flow perturbation effects of the previous design by mounting the three coils on a single support rod. Cylindrical boundary correction factors are computed and compared with experimental data taken in cylinders of quiescent electrolyte and the results are found to agree within 10 percent.

(70 pages)

# CHAPTER I

# INTRODUCTION

Many investigators agree that meaningful measurements of the properties of an equilibrium plasma are extremely difficult to obtain due, in part, to the energetic nature of the plasma stream and to the ability of the ionized gas to conduct an electrical current. Some mass-average properties may be measured by means of interferometry and absorption or emission spectroscopy techniques using instruments that are external to the plasma. However, the problem becomes much more complicated when local property values are measured with internal or immersible probes.

In the design and testing of constricted-arc plasma facilities and magnetohydrodynamic generators and accelerators, two plasma properties are of extreme importance: scalar electrical conductivity and stream velocity. If an instrument could measure conductivity and velocity profiles, then this information could be used to determine the effectiveness of seeding gases and the optimum location of electrodes. Furthermore, since the values of two independent intensive properties are sufficient to determine the thermodynamic state of an equilibrium plasma, a conductivity and, say, a temperature profile could be used with appropriate formulae to obtain local values of several other properties

such as electron density or average electron collision frequency.

This paper is concerned with a particularly convenient configuration of a three-coil conductivity/velocity plasma instrument. Rossow and Posch (1966) designed and tested a probe that consisted of one primary and two secondary coils, each of which was mounted in special geometrical locations on separate support rods. The present work is based on a symmetric coaxial arrangement of the three coils on a single sting or support rod. In a non-conducting medium, the oscillating power supplied to the primary coil, which is equidistant from the two secondary coils, creates a time-varying primary magnetic dipole field. When the device is immersed in a conducting non-quiescent medium, the primary field is perturbed by the induced currents and these perturbations cause changes in the potentials induced at the secondary coils. By means of the theoretical analysis of Rossow and Posch (1966) the change in the sum of the secondary signals may be linearly related to electrical conductivity and the differential secondary output may be related to the product of the electrical conductivity and velocity of the surrounding medium.

The theory of Rossow and Posch (1966) was limited to an unbounded fluid having a uniform conductivity and velocity. In addition, the analysis was restricted to a probe system and conducting medium such that the magnetic Reynolds number was of the order of $10^{-1}$ or less.

Vendell (1968) extended the theory to the case of a cylindrical stream of infinite extent and also presented a data reduction technique to remove the restriction on uniform conductivity and velocity.

This investigation consists of an application of the previous analysis to the coaxial probe configuration. Accordingly, Chapter II contains a brief review of some earlier investigations as well as an account of the work by Rossow, Posch, and Vendell.

Cylindrical boundary correction factors are derived, computed, and presented in Chapter III. Four coaxial probes were assembled and tested in plexiglas cylinders filled with conducting quiescent electrolytes and Chapter IV presents a comparison of the results of these tests with the numerical calculations of Chapter III. Finally, concluding remarks on the merits and possible future applications of the coaxial three-coil plasma probe are made in Chapter V.

# CHAPTER II

## PREVIOUS INVESTIGATIONS

In this chapter, several conductivity and velocity measurement techniques developed in the past are briefly reviewed. The three-coil, non-coaxial, immersible conductivity/velocity plasma probe developed and tested by Rossow and Posch (1966) is discussed in a slightly greater detail. The last section is devoted to a discussion of the extension of the theory of Rossow and Posch (1966) by Vendell (1968).

An electrical conductor is defined as a material that obeys the modified Ohm's law

$$\overline{J} = \sigma \overline{E}$$

where $\overline{J}$ is the current density vector, $\overline{E}$ is the applied field intensity vector, and the electrical conductivity, $\sigma$, is a property of the material. Most metals and electrolytes obey this form of Ohm's law.

A conductivity probe based on Ohm's law is known as a Langmuir probe. Such a probe, however, cannot conveniently be used to measure the electrical conductivity of an ionized medium because of the complex thermal and momentum boundary layer effects, electrical sheaths, contact potentials and the Hall effect. All of these factors must be accounted for

in any theoretical or experimental Langmuir probe investigation.

These difficulties can be overcome to a certain extent by using an electrodeless plasma probe. Various techniques which have been suggested in the past utilize the principle that a magnetic field is distorted by conductivity and motion of a plasma or that the ohmic resistance of a conducting fluid dissipates power from an oscillating magnetic field. However, the coil arrangements used in most of these devices with the exception of that of Rossow and Posch (1966), were such that the measured conductivity and velocity represented values that were averaged over a bulk volume of the fluid under investigation.

Several conductivity measuring devices (Luther, 1963; Lin, Resler, and Kantrowitz, 1955; Fuhs, 1964; and Proberezhskii, 1964) are based on the principle that a small search coil can be used to sense the perturbation caused by a plasma stream of the magnetic field produced by a solenoid. The relative motion can be produced in two different ways: (1) supplying the solenoid with direct current and letting the plasma move through the core of the solenoid (Lin, Resler, and Kantrowitz, 1955), (2) supplying the solenoid with alternating current in which case plasma may or may not be in motion (Luther, 1963; Fuhs, 1964; and Proberezhskii, 1964). The necessary theories have been developed to infer the values of conductivity and velocity of the plasma from the signal induced on the search

coil. The search coil may be immersible (Luther, 1963) or external (Lin, Resler, and Kantrowitz, 1955; Fuhs, 1964; and Proberezhskii, 1964).

Another basic technique (see, for example, Blackman, 1959; Donskoi, Dunaev, and Prokofev, 1963; Akimov and Koneko, 1966; Tanaka and Hagi, 1964; and Savic and Boult, 1962) employs a tuned L-C network in which a solenoid is used as an active inductance element. The network has a certain resonant frequency, $f_o$, and quality factor, $Q_o$, with an air-core test solenoid. The passage of a plasma stream through the solenoid changes the effective impedence which, in turn, changes the resonant frequency by $\Delta f$ and quality factor by $\Delta Q$. The device can then be calibrated to obtain the value of conductivity $\sigma$ from $\Delta f/f_o$ or $\Delta Q/Q_o$.

In another method (Persson, 1961; and Korvitz and Keck, 1964) two identical, single-layer, air-core solenoids are used as active elements of a symmetric RF bridge. When a plasma stream is introduced in one of these solenoids, the bridge becomes unbalanced. The bridge can then be calibrated to obtain the average value of conductivity from the unbalance. The power supply may be sinusoidal (Korvitz and Keck, 1964) or pulsed (Persson, 1961).

The method first used by Olson and Lary (1962) and later modified by Stubbe (1966) is based on the principle that a conducting medium is capable

of dissipating a small amount of power from an oscillating magnetic field which is produced by supplying alternating current to a small immersible coil. The induced e.m.f. produces induced currents in the surrounding conducting medium. The average conductivity of the surrounding medium can be inferred from the power dissipated due to ohmic heating.

As is the case with conductivity measurement techniques, the use of conventional velocity measurement techniques to high speed plasma streams necessitates numerous modifications and a careful analysis of several possible sources of error such as shock waves and relaxation phenomena. A plasma pitot tube capable of measuring the Mach number profile of a plasma stream has been developed, constructed, and tested by Barkan and Whitman (1966). Techniques such as photographing the trajectories of injected sparks have also been used (Carter, et al., 1966).

The first practical means of measuring local conductivity and velocity of a plasma stream has been developed and tested by Rossow and Posch (1966). A brief discussion of the technique has been included in Chapter I. The theory of Rossow and Posch (1966) has been developed with the following basic assumptions. If the flow field is unbounded and has uniform conductivity and velocity and if the applied field is less than $10^{-2}$ gauss justifying the assumption of scalar conductivity, then the resultant magnetic

field can be represented by a power series expansion in magnetic Reynolds number based on the assumption of low values of $R_m$. Typical values of $R_m$, for a constricted-arc wind-tunnel range from $10^{-4}$ to $10^{-1}$.

The probe of Rossow and Posch has the following advantages. It yields local values of conductivity and velocity. The heat-flux sensitivity and flow perturbation problems are significantly reduced as compared to the previously suggested immersible devices. Without losing sensitivity, a lower impressed frequency can be used, thus decreasing stray capacitance effects. The simplicity of the probe configuration offers a very easy fabrication, construction, and assembly of the instrument. Finally, the instrument can be calibrated for conductivity and velocity measurements without using any conducting solids, liquids, or gases.

Vendell (1968) modified the theory of three-sting model of immersible probe of Rossow and Posch (1966) to account for the presence of a finite cylindrical boundary. Outside the boundary, the conductivity of the medium is assumed to be zero and hence no induced electrical currents can exist there. The presence of the boundary is accounted for in terms of conductivity/velocity correction factors. Expressions for the correction factors are derived from the theory developed by Rossow and Posch. The resulting complicated triple-integral expressions were computed numerically using a Gaussian quadrature computer program. Experimental data taken in

cylindrical containers of electrolytes differed by less than 10 percent from analytical values except near the edge of the cylindrical boundary where the induced potential on the conductivity coil was extremely sensitive to the alinement of the probe's axis with the axis of the container. Finally, a method was developed to obtain the conductivity and velocity profiles of axisymmetric plasma jets from the raw data obtained by the probe. The results compared favorably with estimates made by other means (Stine, Watson, and Shepard, 1964).

# CHAPTER III

# THEORY OF THE INSTRUMENT

The first section of this chapter is concerned with a brief review of the theory developed by Rossow and Posch (1966) for a non-coaxial, three-coil, conductivity/velocity plasma probe. The theory was developed on the assumptions that the medium was unbounded, had uniform conductivity, uniform velocity, and low magnetic Reynolds number. The second section contains a discussion of the paper by Vendell (1968) who modified the previous probe theory to include the case of a cylindrically bounded medium having non-uniform conductivity and velocity. The modifications were presented in the form of boundary correction factors that applied to a particular probe configuration having each of the three coils on a separate support rod. The final section contains the principle contribution of this investigation which is the derivation, calculation, and presentation of cylindrical boundary correction factors for a more convenient, coaxial arrangement of the three-coil device. The experimental verification of these calculations is presented in Chapter IV.

## Theory of Rossow and Posch

Rossow and Posch begin their theoretical investigation with Maxwell's equations of electromagnetism

$$\overline{\nabla} \cdot \overline{B} = 0, \tag{1}$$

$$\overline{\nabla} \cdot \overline{E} = 0, \tag{2}$$

$$\overline{\nabla} \times \overline{B} = \mu \overline{J}, \tag{3}$$

$$\overline{\nabla} \times \overline{E} = - \frac{\partial \overline{B}}{\partial t}, \tag{4}$$

the simplified form of Ohm's law

$$\overline{J} = \sigma (\overline{E} + \overline{U} \times \overline{B}), \tag{5}$$

the charge conservation equation for a neutral plasma

$$\overline{\nabla} \cdot \overline{J} = 0, \tag{6}$$

and the Coulomb or transverse gage condition

$$\overline{\nabla} \cdot \overline{A} = 0, \tag{7}$$

where $\overline{A}$ is a vector potential function such that

$$\overline{B} = \overline{\nabla} \times \overline{A}. \tag{8}$$

In these equations, $\overline{B}$ is the magnetic induction vector, $\overline{E}$ is the electric field intensity vector, $\overline{J}$ is the electric current density vector, $\sigma$ is the scalar electrical conductivity, $\overline{U}$ is the stream velocity vector, and $\mu$ is the magnetic permeability of the medium. Vendell (1967) has justified the omission of the displacement current term from Equation (3) above.

Rossow and Posch (1966) obtained a solution to these equations under the following assumptions:

1. The plasma stream extends to infinity in all directions.

2. The flow field has uniform conductivity and velocity.

3. The magnetic field produced by the oscillating power supplied to the primary coil, $\overline{B}_p$, is the only externally applied magnetic field. Furthermore, it is also assumed that this field may be approximated by an ideal point magnetic dipole field.

4. Under the influence of large externally applied magnetic fields, the electrical conductivity of a plasma must be represented by a tensor However, since the externally applied magnetic fields in the work of Rossow and Posch (1966) as well as in the present investigation are small (of the order of $10^{-2}$ gauss), the representation of the conductivity by a scalar quantity is justified.

5. If the magnitude of the magnetic field applied to a conducting medium is small and if the magnetic Reynolds number, $R_m = \sigma \mu U l$,

for the plasma stream is less than unity, then it can be shown that the resultant magnetic field, $\overline{B}$, can be represented by a power series expansion in the magnetic Reynolds number. Such a representation was used in the analysis of Rossow and Posch and, because $R_m$ varies from $10^{-4}$ to $10^{-1}$ for many constricted-arc wind-tunnels, terms of order $R_m^2$ were assumed negligibly small. This assumption is also made in the present work.

6. Relativistic effects are assumed to be negligibly small.

As mentioned above, the primary magnetic field is approximated by an ideal point magnetic dipole field. The magnetic vector potential, $\overline{A}_p$, for an ideal dipole magnetic field in a medium of constant magnetic permeability, $\mu$, and zero conductivity is given by (see, for example, Stratton, 1941)

$$\overline{A}_p (x, y, z, t) = \frac{\mu}{4\pi} \overline{m} \times \overline{\nabla} \left(\frac{1}{r}\right)$$

where (9a)

$$r = (x^2 + y^2 + z^2)^{1/2}$$

and $\overline{m}$ is the magnetic dipole moment. For the primary coil alined parallel to the z-axis, the magnetic dipole moment, $\overline{m}$, is given by

$$\overline{m} = \overline{k}\, n_p r_p^2 \pi I_p \cos(\omega t) \tag{9b}$$

where $r_p$ is the characteristic radius of the $n_p$-turn primary coil, $I_p$ is the peak electric current, $\omega/2\pi$ is the impressed frequency, and $\overline{k}$ is a unit vector parallel to the z-axis. The last of the fundamental equations used by Rossow and Posch (1966) is the well-known Faraday's law of electromagnetic induction which states that the potential, $\phi_s$, induced on a secondary coil placed anywhere in a resultant magnetic field, $\overline{B}$, is given by

$$\phi_s = -\pi n_s r_s^2 \frac{\partial}{\partial t} (\overline{B} \cdot \overline{N}_s) \tag{10}$$

where $r_s$ is the characteristic radius of the $n_s$-turn secondary coil, and $\overline{N}_s$ is a unit vector alined with the axis of the coil. As an approximation, vector $\overline{B}$ is evaluated at the center of the secondary coil.

The total current density vector, $\overline{J}$, as given by Equation (5) may be divided into two components,

$$\overline{J} = \overline{J}_t + \overline{J}_{\parallel} \tag{11}$$

where

$$\overline{J}_t = \sigma \overline{E}_t \tag{12}$$

and

$$\overline{J}_{\parallel} = \sigma (\overline{U}_{\parallel} \times \overline{B}_p) \tag{13}$$

where $\overline{E}_t$ is the induced electric field intensity vector, $\overline{U}_{\parallel}$ is the plasma stream velocity vector which is assumed to be parallel to the z-axis, and $\overline{B}_p$ is the primary magnetic induction vector. The vector $\overline{J}_t$ is induced by the interaction of the electric field, $\overline{E}_t$, and the quiescent conducting medium whereas the vector $\overline{J}_{\parallel}$ arises from the motion of the conducting fluid across lines of force, $\overline{B}_p$. Equation (3) suggests the existence of perturbation magnetic fields $\overline{b}_t$ and $\overline{b}_{\parallel}$ associated with current density vectors $\overline{J}_t$ and $\overline{J}_{\parallel}$ respectively. Hence, based on the assumptions of small primary magnetic field, $\overline{B}_p$, and magnetic Reynolds number, $R_m$, less than unity (see assumption 5 above) the resultant magnetic field, $\overline{B}$, is

$$\overline{B} = \overline{B}_p + \overline{b}_{\parallel} + \overline{b}_t. \tag{14}$$

Cross coupling between the perturbation fields is of second order in $R_m$ and is neglected here. Rossow and Posch (1966) have obtained a solution

to Equations (1) through (14) for a particular geometrical arrangement of their three-coil model.

## Modified Probe Theory for a Cylindrically Bounded Medium by Vendell

Vendell (1968) extended the theory of Rossow and Posch (1966) to include the case of a cylindrically bounded medium of infinite extent in the positive and negative z-directions having non-uniform conductivity and velocity. Initially, the conductivity and velocity were assumed to be uniform inside the cylinder and zero elsewhere. These assumptions led to the following boundary conditions for the current density vector $\overline{J}$.

$$\overline{J} = 0 \text{ whenever } x^2 + y^2 > R^2 \tag{15}$$

$$\overline{J} \cdot \overline{N}_{\perp} = 0 \text{ whenever } x^2 + y^2 = R^2 \tag{16}$$

where $\overline{N}_{\perp}$ is a unit vector perpendicular to the cylindrical boundary and R is the radius of the cylindrical medium.

Combining Equations (3), (7), and (8), one obtains

$$\nabla^2 \overline{A} = -\mu \overline{J} \tag{17}$$

which has to be solved simultaneously with the Ohm's law, Equation (5) and the boundary conditions specified in Equations (15) and (16) above. Using an analogy based on stream function for a steady, two-dimensional flow of an incompressible fluid, and the method of magnetostatic images, Vendell (1968) obtained the following expression for the two-dimensional current density vector field $\bar{J}_t$.

$$\bar{J}_t = -G_t \left\{ \bar{i} \left[ \frac{R\rho^2 y}{(\rho x + R^2 + \rho^2 y^2 + R^2 z^2)^{3/2}} - \frac{y}{(x + \rho^2 + y^2 + z^2)^{3/2}} \right] - \bar{j} \left[ \frac{R\rho(\rho x + R^2)}{(\rho x + R^2 + \rho^2 y^2 + R^2 z^2)^{3/2}} - \frac{x + \rho}{(x + \rho^2 + y^2 + z^2)^{3/2}} \right] \right\} \tag{18}$$

where $\rho$ is the distance of the probe from the axis of the plasma jet along negative x-direction, and

$$G_t = \sigma \omega m \sin(\omega t) \tag{19}$$

where $\sigma$ is the uniform conductivity, $\omega / 2\pi$ is the impressed frequency and

$$m = \mu n_p r_p^2 I_p / 4 . \tag{20}$$

It should be noted that the current density vector, $\overline{J}_t$, is caused by the application of the induced electric field, $\overline{E}_t$, to the stationary conducting fluid. Equation (3) implies the existence of a perturbation magnetic induction vector, $\overline{b}_t$, caused by the presence of $\overline{J}_t$ such that

$$\overline{\nabla} \times \overline{b}_t = \mu \overline{J}_t . \tag{21}$$

Since $\overline{J}_t$ is known, $\overline{b}_t$ may be obtained from vector Equation (21) and Equation (11)(Stratton, 1941, p. 231) as

$$\overline{b}_t (x', y', z', t) = \frac{\mu}{4\pi} \int_{-\infty}^{\infty} \int_{-R}^{R} \int_{-\sqrt{R^2 - y^2}}^{\sqrt{R^2 - y^2}} \overline{J}_t (x, y, z, t) \times \overline{\nabla}(r^{-1}) \, dx \, dy \, dz \tag{22}$$

where

$r^2 = (x - x')^2 + (y - y')^2 + (z - z')^2$ and $x'$, $y'$, $z'$ are coordinates of any field point. If one substitutes Equation (18) for $\overline{J}_t$ into Equation (22), then the result in dimensionless form will be

$$b_{zt}(X', Y', Z', t) = \frac{\mu G_t}{4\pi R} \int_{-\infty}^{\infty} \int_{-1}^{1} \int_{-\sqrt{1-Y^2}}^{\sqrt{1-Y^2}} \left[ \frac{1}{\left(\overline{X - X'}^2 + \overline{Y - Y'}^2 + \overline{Z - Z'}^2\right)^{3/2}} \right] \times$$

$$\left[ \frac{P^2 Y (Y - Y') + \overline{X - X'}\ P\ \overline{PX + 1}}{\left(\overline{PX + 1}^2 + P^2 Y^2 + Z^2\right)^{3/2}} - \right. \tag{23}$$

$$\left. \frac{\overline{X - X'}\ \overline{X + P} + Y (Y - Y')}{\left(\overline{X + P}^2 + Y^2 + Z^2\right)^{3/2}} \right] dx\, dy\, dz$$

where $X = x/R$, $Y = y/R$, $Z = z/R$, $X' = x'/R$, $Y' = y'/R$, $Z' = z'/R$, and $P = \rho/R$. Because the conductivity secondary coil of the three-sting model is alined parallel to the z-axis, only the z- component of the perturbation field, $b_{zt}$ is given in Equation (23).

The basic equations obtained by Vendell (1968) in an exactly parallel analysis of the primary magnetic field perturbation caused by the motion of a conducting fluid are summarized below.

$$\bar{J}_{\parallel} = -G_{\parallel}\, z \left\{ \left[ 3R^3 \rho^2 y \left( \overline{\rho x + R^2}^{\,2} + \rho^2 y^2 + R^2 z^2 \right)^{-5/2} - 3y \left( \overline{x + \rho}^{\,2} + y^2 + z^2 \right)^{-5/2} \right] \bar{i} - \left[ 3R^3 \rho \left( \overline{\rho x + R^2}^{\,2} + \rho^2 y^2 + R^2 z^2 \right)^{-5/2} - 3(x + \rho) \left( \overline{x + \rho}^{\,2} + y^2 + z^2 \right)^{-5/2} \right] \bar{j} \right\} \tag{24}$$

where

$$G_{\parallel} = \sigma\, U_{\parallel}\, m \cos(\omega t) \tag{25}$$

and as given by Equation (20)

$$m = \mu\, n_p\, r_p^2\, I_p / 4.$$

As was the case with $\overline{b}_t$, $\overline{b}_{\parallel}$ is related to $\overline{J}_{\parallel}$ by the expression

$$\overline{b}_{\parallel}(x', y', z', t) = \frac{\mu}{4\pi} \int_{-\infty}^{\infty} \int_{-R}^{R} \int_{-\sqrt{R^2-y^2}}^{\sqrt{R^2-y^2}} \overline{J}_{\parallel}(x, y, z, t) \times \overline{\nabla}(r^{-1})\, dx\, dy\, dz \tag{26}$$

where, as before, $r^2 = (x - x')^2 + (y - y')^2 + (z - z')^2$. Because the velocity secondary coil of the non-coaxial probe is alined parallel to the y-axis, only the y-component of the perturbation magnetic field, $b_{y\parallel}$, will appear in Faraday's law Therefore, if one substitutes the expression for $\overline{J}_{\parallel}$ from Equation (24) into Equation (26), and non-dimensionlizes the resulting expression with respect to R, then one obtains

$$b_{y\parallel} = -\frac{3\mu G_{\parallel}}{4\pi R^2} \int_{-\infty}^{\infty} \int_{-1}^{1} \int_{-\sqrt{1-Y^2}}^{\sqrt{1-Y^2}} \left[ \frac{YZ^2}{\overline{X - X'}^2 + \overline{Y - Y'}^2 + \overline{Z - Z'}^2} \right] \times \left[ \frac{P^2}{(\overline{PX + 1}^2 + P^2Y^2 + Z^2)^{5/2}} - \frac{1}{(\overline{X + P}^2 + Y^2 + Z^2)^{5/2}} \right] dX\, dY\, dZ. \tag{27}$$

Vendell (1968) applied the above equations to the three-sting probe configuration to obtain the expression for conductivity and velocity correction factors which account for the presence of a cylindrical boundary surrounding the medium. In the next section these equations will be applied to a coaxial probe configuration.

## Analysis of a Three-Coil Coaxial Probe Configuration

The basic details of the coaxial probe are schematically shown in Figure 1. Two identical secondary coils labeled S1 and S2 are mounted symmetrically with respect to a primary coil labeled P on a piece of quartz tubing. The three coils are wound on teflon coil forms and are held in their design positions by teflon spacers. Then, the assembly is inserted into a quartz tubing and secured in its position by additional teflon spacers.

As illustrated by Figure 2, the z-axis of a rectangular cartesian coordinate system coincides with the axis of the cylindrical medium and the axis of the support rod is alined parallel to the z-axis. The center of the primary coil lies on the x-axis. The secondary coils S1 and S2 lie at a distance d from the primary coil along positive and negative z-direction respectively. The distance of the probe from the z-axis along negative x-direction is denoted by $\rho$, whereas the radius of the cylindrical medium is represented by R. Throughout the present

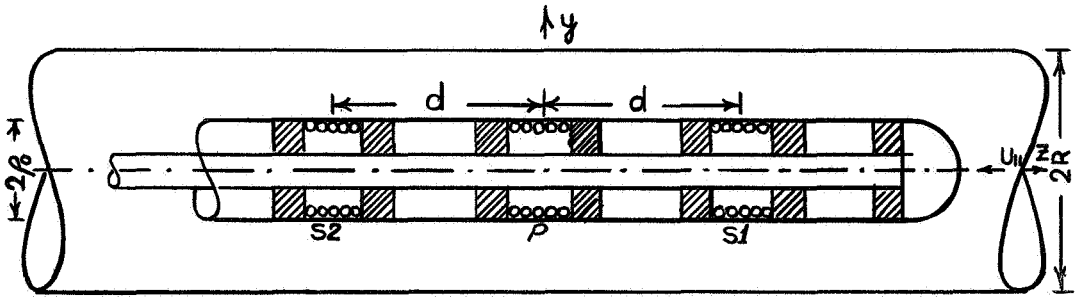


Figure 1. Schematic sketch of the three-coil coaxial, conductivity velocity plasma probe.

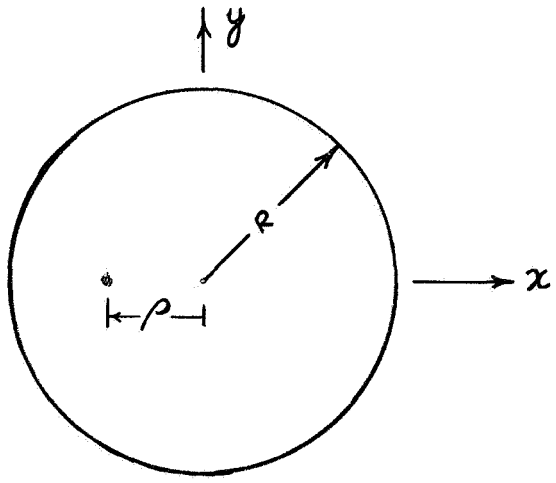


Figure 2. Schematic sketch showing the position of the probe inside the cylindrical boundary.

investigation it will be assumed that the conducting medium has a uniform velocity $U_{\parallel}$ along negative z-direction.

The primary coil is supplied with an oscillating power of one watt at a frequency of 100 kHz. When the probe is in room air, due to electromagnetic coupling between the primary and the secondary coils, and to the symmetrical arrangement of the three coils, identical potentials are induced on the two secondary coils. Therefore, the difference of the potential outputs, in room air, is theoretically zero whereas the sum of the potential outputs is a non-trivial quantity. This output potential sum is nulled or cancelled out with the help of a nulling system consisting of tickler coils (for details see Vendell, 1967, p. 21-22).

If the probe, after having been nulled, is immersed in a moving conducting medium, then the primary magnetic field, $\overline{B}_p$, is perturbed by the conductivity and motion of the medium. The induced potentials on the two secondary coils are such that their sum, $\phi_{\Sigma}$, and the difference, $\phi_{\Upsilon}$ , are linearly dependent upon the electrical conductivity, $\sigma$, and the product of conductivity and velocity, $\sigma U_{\parallel}$ , respectively. In the sequel, therefore, the perturbation potential outputs $\phi_{\Sigma}$ and $\phi_{\Upsilon}$ will be referred to by potential-sum and potential-difference respectively. The signals $\phi_{\Sigma}$ and $\phi_{\Upsilon}$ are displayed respectively, on the upper and lower beam of a dual-beam cathode-ray oscilloscope.

Electrical conductivity

The z-component of the time-dependent perturbation magnetic field $b_{zt}$, caused by the presence of current loops $\bar{J}_t$ is given by Equation (23). If one substitutes (-P, O, D) for (X', Y', Z') in Equation (23), then one obtains the following expression for $b_{zt}$ at the center of the secondary coil, S2.

$$b_{zt}(-P, O, D, t) = \frac{\mu G t}{4\pi R} \int_{-\infty}^{\infty} \int_{-1}^{1} \int_{-\sqrt{1-Y^2}}^{\sqrt{1-Y^2}} \left[ \frac{1}{(\overline{X+P}^2 + Y^2 + \overline{Z-D}^2)^{3/2}} \right] \times \left[ \frac{P^2 Y^2 + \overline{X+P}\, P\, \overline{PX+1}}{(\overline{PX+1}^2 + P^2 Y^2 + Z^2)^{3/2}} \right] - \left[ \frac{\overline{X+P}^2 + Y^2}{(\overline{X+P}^2 + Y^2 + Z^2)^{3/2}} \right] dX\, dY\, dZ \tag{28}$$

where, as mentioned earlier, $P = \rho/R$ is the radial position parameter, $D = d/R$ is the coil spacing parameter, and $G_t$ is given by Equation (19). Substitution of this expression for $b_{zt}$ into Faraday'law, Equation (10)

yields the following expression for the perturbation potential—sum,

$$\phi_{\Sigma} = - \frac{\pi n_s r_s^2 \mu \sigma \omega^2 m \cos(\omega t)}{2 \pi R} \int_{-\infty}^{\infty} \int_{-1}^{1} \int_{-\sqrt{1 - Y^2}}^{\sqrt{1 - Y^2}} F_{\Sigma} \, dx \, dy \, dz \tag{29}$$

where $F_{\Sigma}$ denotes the complicated integrand of Equation (28). Note that $G_t$ has been replaced by its equivalent expression $G_t = \sigma \omega m \sin(\omega t)$ and m is given by Equation (20).

Next, an expression for the induced perturbation potential-sum, $\phi_{\Sigma\infty}$, when the probe is immersed in an unbounded, quiescent medium of uniform conductivity will be obtained. This analysis begins with the following expression for the perturbation magnetic induction vector $\bar{b}_t$ produced by an ideal magnetic dipole in an infinite conducting medium which has been derived in Rossow and Posch (1966).

$$\bar{b}_{t\infty} = \frac{\sigma \mu \omega m}{2} \sin(\omega t) \left[ \bar{i} \frac{xz}{r^3} + \bar{j} \frac{yz}{r^3} + \bar{k} \frac{r^2 + z^2}{r^3} \right] \tag{30}$$

The origin of the coordinate system coincides with the point magnetic dipole. If one takes the z-component of vector $\bar{b}_{t\infty}$, substitutes $(\rho, 0, d)$ for $(x, y, z)$, then one obtains

$$b_{zt\infty} = -\frac{\sigma \mu \omega m \sin(\omega t)}{d} \quad . \tag{31}$$

Substitution of this expression in Faraday's law, Equation (10) results in

$$\phi_{\Sigma\infty} = 2 \pi n_s r_s^2 \frac{\sigma \mu \omega^2 m \cos(\omega t)}{d} \tag{32}$$

where $\phi_{\Sigma\infty}$ is the perturbation potential-sum induced in an infinite medium.

The conductivity correction factor, $\theta_\Sigma$, is defined as the ratio of the potential-sum induced in a finite cylindrical region having a uniform conductivity to the potential-sum induced in an infinite region having the same uniform conductivity. Division of Equation (29) by Equation (32) eliminates the probe and coil characteristics and yields the following expression for $\theta_\Sigma$.

$$\theta_\Sigma \equiv \frac{\phi_\Sigma}{\phi_{\Sigma\infty}} = -\frac{D}{4\pi} \int_{-\infty}^{\infty} \int_{-1}^{1} \int_{-\sqrt{1-Y^2}}^{\sqrt{1-Y^2}} F_\Sigma \, dX \, dY \, dZ \tag{33}$$

Discussion of the use of $\theta_\Sigma$ to reduce the raw data to obtain the value of electrical conductivity, $\sigma$, is deferred to the last section of this Chapter.

Product of conductivity and velocity or $\sigma U_{||}$

The time-dependent perturbation magnetic field, $\overline{b}_{||}$ , caused by the presence of current loops $\overline{J}_{||}$ is given by Equations (26) and (24). Since the axis of the secondary coils is alined parallel to z-axis, therefore only z-component of $\overline{b}_{||}$ will appear in Faraday's law, Equation (10). When this component, $b_{||z}$, is evaluated at the center of the secondary coil S2 whose coordinates are $(x', y', z') = (-\rho, o, d)$ and the resulting expression in non-dimensionalized with respect to R, one obtains

$$b_{z||}(-P, O, D) = \frac{-3\mu G_{||}}{4\pi R^2} \int_{-\infty}^{\infty} \int_{-1}^{1} \int_{-\sqrt{1-Y^2}}^{\sqrt{1-Y^2}} \left[ \frac{Z}{(\overline{X+P}^2 + Y^2 + \overline{Z-D}^2)^{3/2}} \right] X$$

$$\left[ \frac{P^2 Y^2 + P\,\overline{X+P}\;\overline{PX+1}}{(\overline{PX+1}^2 + P^2 Y^2 + Z^2)^{5/2}} - \frac{\overline{X+P}^2 + Y^2}{(\overline{X+P}^2 + Y^2 + Z^2)^{5/2}} \right] dX\, dY\, dZ \tag{34}$$

If the complicated integrand is denoted by $F_T$ and if Equation (34) is rewritten, then the result is

$$b_{z\|}(-P, O, D) = -\frac{3\mu G_{\|}}{4\pi R^2}\int_{-\infty}^{\infty}\int_{-1}^{1}\int_{-\sqrt{1-Y^2}}^{\sqrt{1-Y^2}} F_T \, dX \, dY \, dZ \tag{35}$$

where

$$G_{\|} = \sigma U_{\|} \, m \cos(\omega t)$$

and

$$m = \mu n_p r_p^2 I_p/4 .$$

Substitution of the above expression for $b_{z\|}$ in Faraday's law, Equation (10) yields the following expression for the perturbation potential-difference, $\phi_T$.

$$\phi_T = -\frac{3 n_s r_s^2 \mu\sigma U_{\|} \, m \omega \sin(\omega t)}{2R^2}\int_{-\infty}^{\infty}\int_{-1}^{1}\int_{-\sqrt{1-Y^2}}^{\sqrt{1-Y^2}} F_T \, dX \, dY \, dZ \tag{36}$$

The expression for the magnetic field perturbation brought about by a conducting unbounded uniform stream, $\bar{b}_{\|\infty}$, is given by Equation (16) in Rossow and Posch (1966) as

$$\bar{b}_{\parallel \infty} = 1/2\ \sigma \mu U_{\parallel}\ m \cos(\omega t)\ \left[1 - (3z^2/r^2)\right] \times$$

$$\left[\bar{i}(x/r^3) + \bar{j}(y/r^3) + \bar{k}(z/r^3)\right] \tag{37}$$

Note that the origin of the coordinate system coincides with the point magnetic dipole and $r = (x^2 + y^2 + z^2)^{1/2}$. Taking the z-component of $\bar{b}_{\parallel \infty}$ and evaluating it at the center of the secondary coil S2 given by $(x, y, z) = (0, 0, d)$ it can be shown that

$$b_{z \parallel \infty}(0, 0, d) = -\frac{\sigma \mu U_{\parallel}\ m \cos(\omega t)}{d^2} \tag{38}$$

From Equation (38) above and Faraday's law, Equation (10) one can readily obtain

$$\phi_{T \infty} = 2 \pi n_s r_s^2 \sigma \mu U_{\parallel} m \omega \sin(\omega t)/d^2 \tag{39}$$

where $\phi_{T \infty}$ is the perturbation potential-difference induced in an infinite medium.

The correction factor $\theta_T$ is defined as the ratio of potential-difference $\phi_T$, induced in a finite cylindrical region having uniform conductivity, $\sigma$, and uniform velocity, $U_{\parallel}$, to the potential-difference

$\phi_{T\infty}$, induced in an infinite region having the same uniform conductivity and velocity. Although as suggested by Equations (36) and (39) this correction factor applies to the product $\sigma U_{\parallel}$, yet, for the sake of convenience, it will hereafter be referred to as the velocity correction factor. Division of Equation (36) by Equation (39) eliminates the probe and coil characteristics and results in

$$\theta_T = \frac{\phi_T}{\phi_{T\infty}} = -\frac{3D^2}{4\pi} \int_{-\infty}^{\infty} \int_{-1}^{1} \int_{-\sqrt{1-Y^2}}^{\sqrt{1-Y^2}} F_T \, dX \, dY \, dZ. \tag{40}$$

Discussion of the use of $\theta_T$ in obtaining the value of stream velocity, $U_{\parallel}$, from the raw data is contained in the last section of this chapter.

Numerical evaluation of boundary correction factors

Closed-form solutions to the complicated integrals in the expressions for $\theta_\Sigma$ and $\theta_T$ could not be obtained. Therefore, values of $\theta_\Sigma$ and $\theta_T$ were computed numerically using a Gaussian quadrature computer program. These analytical results are presented graphically in Figures 3 through 5. Figure 3 is a plot of the conductivity correction factor $\theta_\Sigma = \phi_\Sigma / \phi_{\Sigma\infty}$ versus the coil spacing parameter, $D = d/R$, for five different values of the radial position parameter, $P = \rho / R$. Dashed portions of the curves represent extrapolations. Figure 4 is a plot of $\theta_\Sigma$ and $\theta_T$, correct to

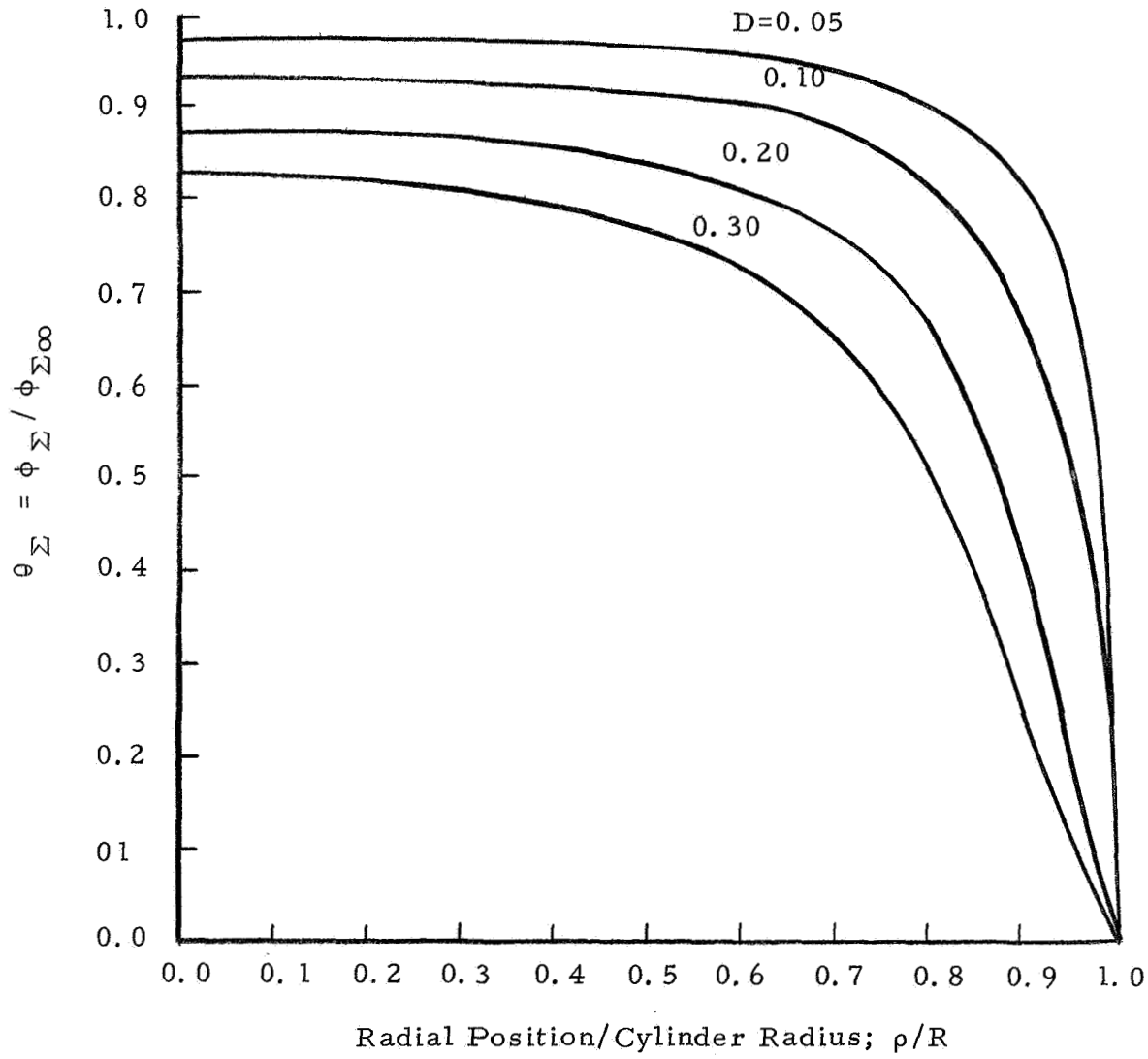


Figure 3. Conductivity boundary correction factor $\theta_\Sigma$ as a function of the radial position parameter P for several typical values of the coil spacing parameter D = d/R.

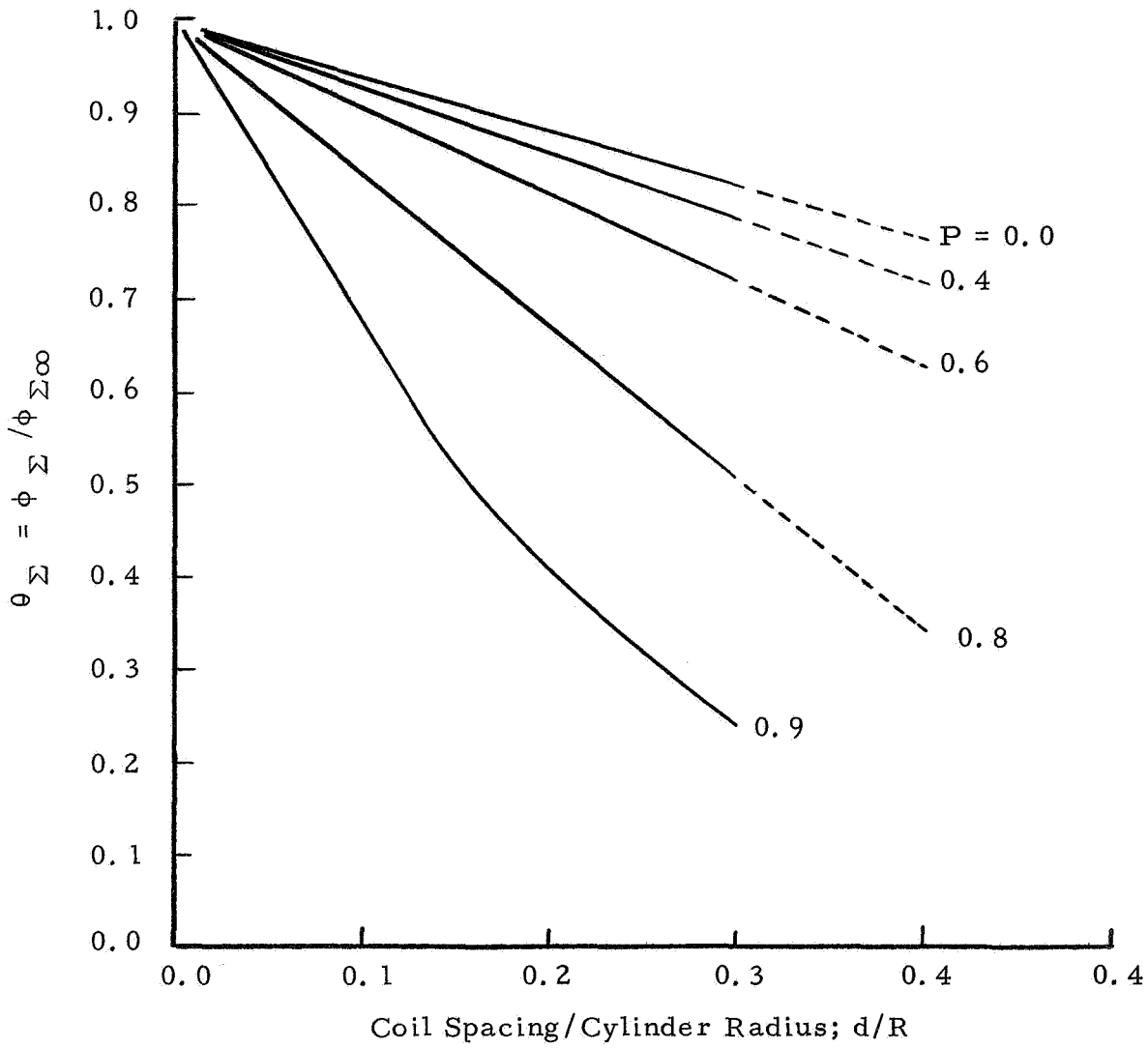


Figure 4. Conductivity boundary correction factor $\theta_\Sigma$ as a function of the coil spacing parameter D for several typical values of the radial position parameter $P = \rho/R$.

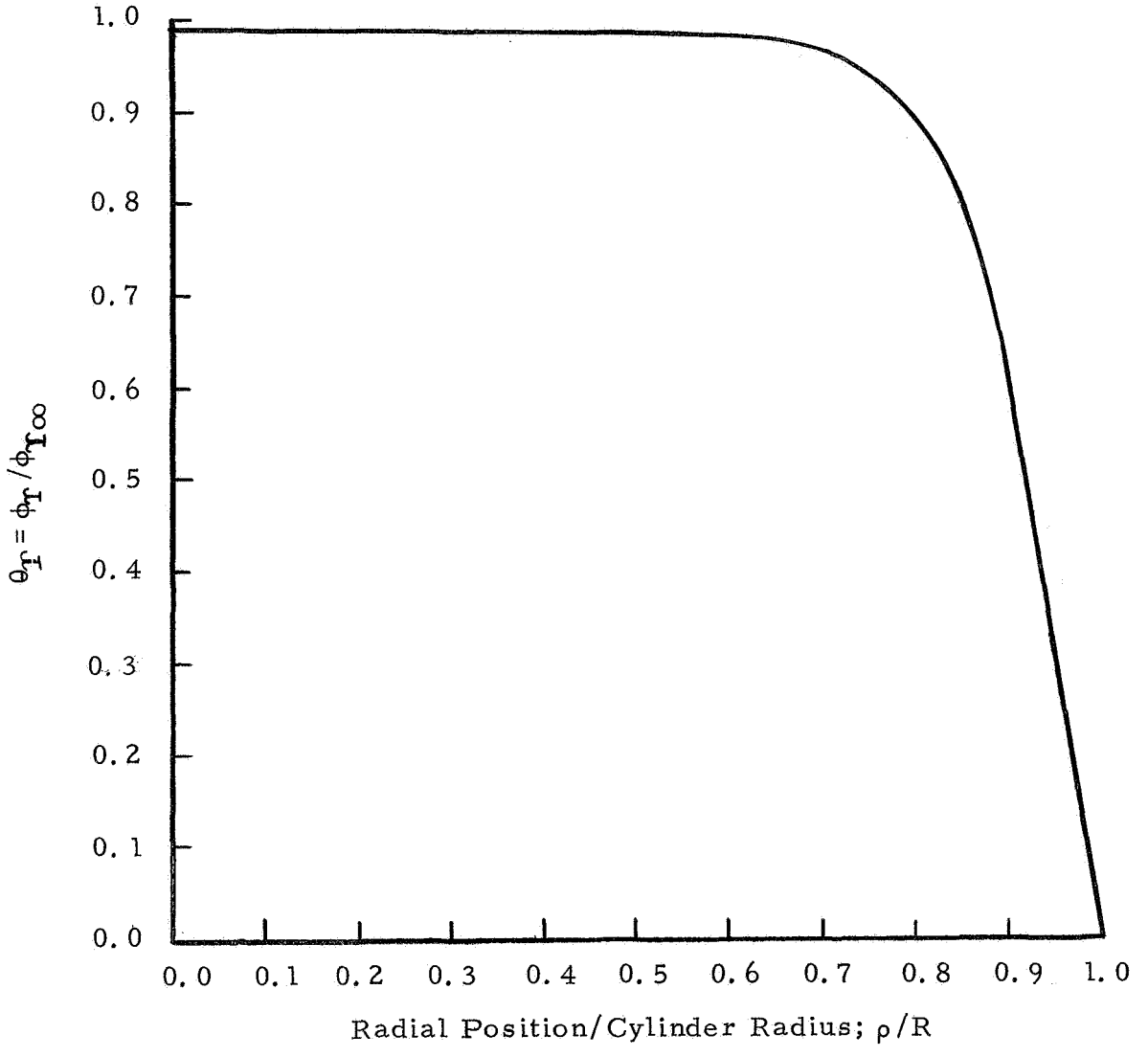


Figure 5. Velocity boundary correction factor $\theta_T$ as a function of radial position for the case D=d/R= 0.30.

three significant figures, are presented in tabular form in Tables 1 and 2.

Table 1. Conductivity correction factors $\theta_{\Sigma}$

| $P = \rho/R$ | $D = d/R$ | | | |
|---|---|---|---|---|
| | 0.05 | 0.10 | 0.20 | 0.30 |
| 0.0 | .971 | .941 | .885 | .824 |
| 0.4 | .964 | .928 | .859 | .792 |
| 0.6 | .953 | .905 | .813 | .723 |
| 0.8 | .915 | .830 | .663 | .514 |
| 0.9 | .836 | .673 | .403 | .242 |

Table 2. Velocity correction factors $\theta_{\Upsilon}$

| $D = d/R$ | $P = \rho/R$ | | | | |
|---|---|---|---|---|---|
| | 0.0 | 0.6 | 0.7 | 0.8 | 0.9 |
| 0.3 | .990 | .983 | .968 | .906 | .626 |

As indicated by Figures 3 and 4, $\theta_{\Sigma}$ has a nearly linear dependence upon P for a given D whenever $P \leq 0.8$ and $D \leq 0.3$. There is a sudden decrease in the value of $\theta_{\Sigma}$ near the edge of the stream, particularly

for low values of D. It is evident from Figure 3 that the data obtained with a probe having a small coil-spacing d in a large diameter stream needs practically no correction for the presence of the cylindrical boundary except at points very close to the edge of the stream. As suggested by Figure 5, the deviation of $\theta_T$ from unity is negligibly small whenever $P \leq 0.7$ and $D \leq 0.3$. Consequently, more values of $\theta_T$ were not computed because of the cost involved in carrying out the numerical integrations.

A comparison of the values of the correction factors $\theta_\Sigma$ and $\theta_T$ for the coaxial probe and the three-sting model (see Vendell, 1967) reveals that the values of $\theta_\Sigma$ and $\theta_T$ for the coaxial configuration are closer to unity than the corresponding values for the three-sting configuration. In particular, for the coaxial probe, the correction to be applied to reduce the raw velocity data is negligible for all practical purposes.

Hub correction factors

The presence of the non-conducting quartz tubing which protects the probe from the hot plasma eliminates some of the induced electric current loops assumed to exist in the derivations of the expressions for $\theta_\Sigma$ and $\theta_T$. The absence of these currents results in a reduced magnitude of the induced potential-outputs. Therefore, correction factors have to be applied to both conductivity and velocity to account for the presence of

the heat shields. In the sequel, these correction factors will be referred to as the hub correction factors and denoted by $\sigma_{true}/\sigma$ and $U_{\parallel\ true}/U_{\parallel}$ for the case of conductivity and velocity respectively.

Equation (29) indicates a linear dependence of $\phi_{\Sigma}$ on the conductivity $\sigma$. As discussed earlier, $\phi_{\Sigma}$ is the induced potential-sum caused by the presence of current loops, $\overline{J}_t$, in the cylindrical region of radius R extending to infinity along positive and negative z-direction. Therefore, if one replaces R by $\rho_0$ in Equation (29), then one obtains the value of $\phi_{\Sigma\,\rho_0}$, which would have been induced by the electric currents which would have been present in the region now occupied by the quartz tubing of radius $\rho_0$ (see Figure 1). Since the quartz tubing extends on either side of the primary coil to a distance large enough to include any measurable signal loss, the assumption that the quartz tubing extends to infinity along its axial direction is justified. Furthermore, because the idealized point magnetic dipole is assumed to lie on the axis of the support rod, it is obvious that P = 0 - 0 in Equation (29). Suggested by the linear dependence of conductivity, $\sigma$, on $\phi_{\Sigma}$, the conductivity hub correction factor is defined as

$$\frac{\sigma_{true}}{\sigma} = \frac{\phi_{\Sigma\infty}}{\phi_{\Sigma\infty} - \phi_{\Sigma\,\rho_0}}$$

which on simplification becomes

$$\frac{\sigma_{true}}{\sigma} = \frac{1}{1 - \theta_{\Sigma}} \quad . \tag{41}$$

In this expression, the governing parameters of $\theta_{\Sigma}$ take on the values $P = 0.0$ and $D = d/\rho_0$.

As was the case with conductivity, the linear dependence of $\phi_T$ on the product of conductivity and velocity, $\sigma U_{\parallel}$ , indicated by Equation (39) suggests the following definition of hub correction factor for velocity.

$$\frac{(\sigma U_{\parallel})_{true}}{(\sigma U_{\parallel})} = \frac{\phi_{T\infty}}{\phi_{T\infty} - \phi_{T\rho_0}}$$

which on simplification becomes

$$\frac{U_{\parallel\, true}}{U_{\parallel}} = \frac{1 - \theta_{\Sigma}}{1 - \theta_{T}} \quad . \tag{42}$$

Note that in Equation (42) $P = 0.0$ and $D = d/\rho_0$. A plot of analytical values of $\sigma_{true}/\sigma$ and $U_{\parallel\, true}/U_{\parallel}$ versus the dimensionless parameter $2\,\rho_0/d$ is shown in Figure 6.

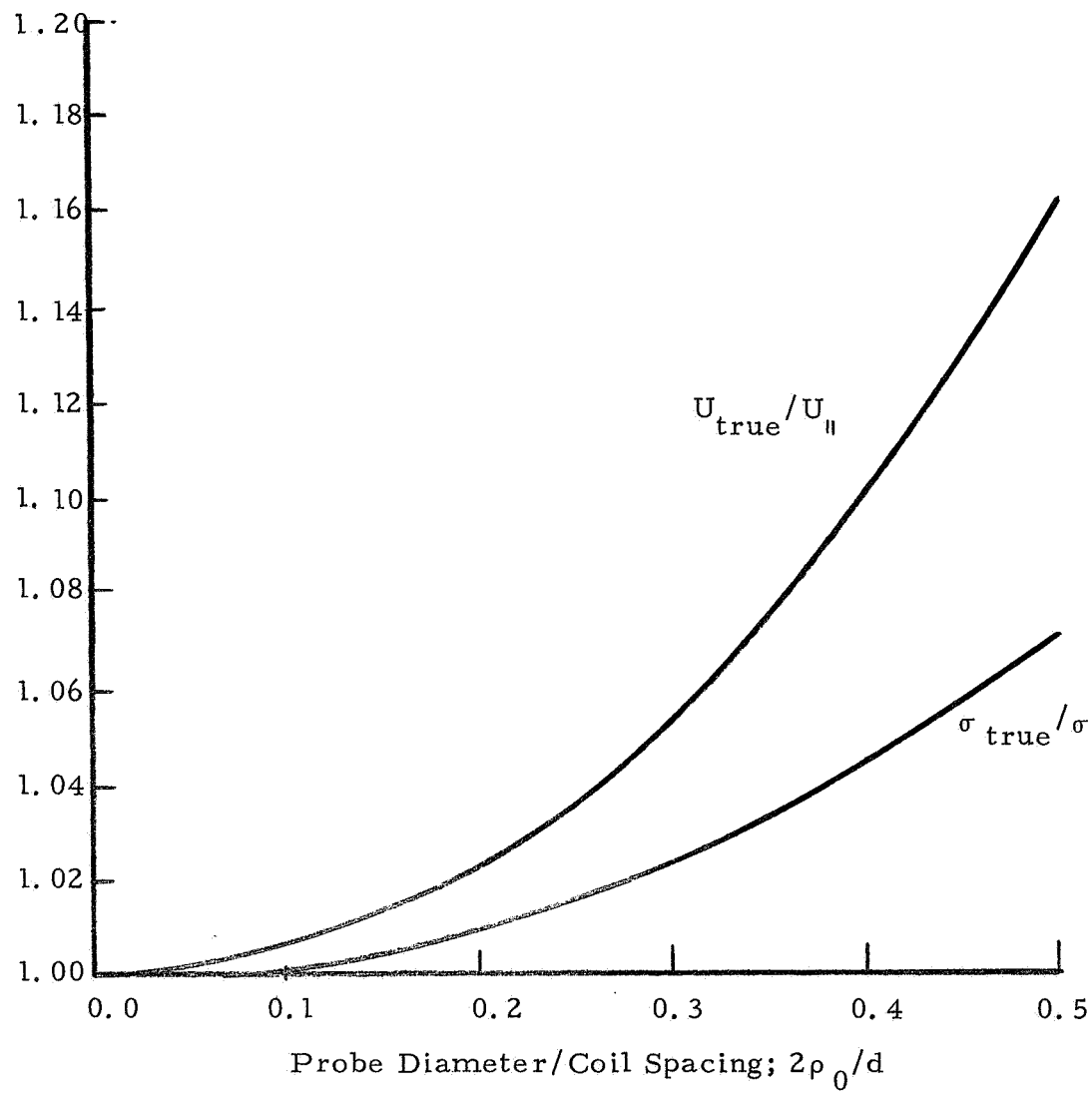


Figure 6. Conductivity and velocity hub correction factors that compensate for the perturbation current loops which cannot exist in the region occupied by the coaxial probe.

## Calibration Equations for the Coaxial Probe

In this section a method of calibrating the coaxial probe for both the electrical conductivity, $\sigma$ , and the stream velocity, $U_{||}$ , is discussed. The discussion also includes the application of the cylindrical boundary correction factors, $\theta_{\Sigma}$ and $\theta_{T}$ , as well as the hub correction factors, $\sigma_{true}/\sigma$ and $U_{||\,true}/U_{||}$ , to obtain the corrected values of $\sigma$ and $U_{||}$ .

The analysis begins with the derivation of an expression for calibration potential, $\phi_{\Sigma\,cal}$, which is the sum of the potentials induced on the two secondary coils when the probe is operated in room air, at least 15 cm away from any conducting or dielectric medium. The idealized magnetic dipole field of the primary coil is given by Equation (4) of Vendell (1966) as

$$\overline{B}_p = - m \cos(\omega t) \left[ \overline{i} \frac{3xz}{r^5} + \overline{j} \frac{3yz}{r^5} + \overline{k} \left(\frac{3z^2}{r^2} - 1\right)/r^3 \right] \tag{43}$$

where $m = n_p r_p^2 I_p/4$ and $r = (x^2 + y^2 + z^2)^{1/2}$ . The cartesian coordinates (x, y, z) are referred to the origin coincidental with the center of the primary coil. The secondary coils S1 and S2 are located at (0, 0, d) and (0, 0, -d) respectively. With the probe in room air, the z-component of the primary magnetic field, $B_{pz}$, at the center of either of the secondary

$$B_{pz} = -\frac{2\,m\cos(\omega t)}{d^3} \tag{44}$$

Substitution of this expression for $B_{pz}$ into Faraday's law, Equation (10) yields the potential induced on either of the secondary coils. However, since calibration potential, $\phi_{\Sigma\,cal}$, which is displayed on the upper beam of the oscilloscope is the sum of the signals induced on the two secondary coils, therefore the peak-to-peak signal displayed on the scope is given by

$$\phi_{\Sigma\,cal} = 2\,\pi\,n_p\,r_p^2\,n_s\,r_s^2\,\mu\,\omega\,I_p/d^3\,. \tag{45}$$

If the probe is nulled, and immersed in an unbounded conducting medium, then the perturbation potential-sum induced, $\phi_{\Sigma\infty}$, is given by Equation (32). The peak-to-peak signal which will be displayed on the scope is given by

$$\phi_{\Sigma\infty} = 4\,\pi\,n_s\,r_s^2\,\sigma\,\mu\,\omega^2\,m/d. \tag{46}$$

If one divides Equation (45) by Equation (46), one obtains

$$\sigma = \frac{2}{\mu \omega d^2} \quad \frac{\phi_{\Sigma \infty}}{\phi_{\Sigma\, cal}} \quad . \tag{47}$$

Similarly, peak-to-peak perturbation potential-difference, $\phi_{T\infty}$, can be obtained from Equation (39).

$$\phi_{T\infty} = 4 \pi n_s r_s^2 \sigma \mu U_{\parallel} m \omega / d^2 \tag{48}$$

Division of Equation (45) by Equation (48) and subsequent rearrangement of terms yields

$$U_{\parallel} = \omega d \frac{\phi_{T\infty}}{\phi_{\Sigma \infty}} \tag{49}$$

The restriction of an unbounded medium can now be removed by introducing the correction factors $\theta_{\Sigma}$ and $\theta_T$ which account for the presence of a cylindrical boundary surrounding the medium. By definition, $\phi_{\Sigma\infty} = \phi_{\Sigma} / \theta_{\Sigma}$ and $\phi_{T\infty} = \phi_T / \theta_T$. Substitution of these expressions in Equation (47) and (49) results in

$$\sigma = \frac{2}{\mu \omega d^2} \quad \frac{\phi_{\Sigma}}{\phi_{\Sigma\, cal}} \cdot \frac{1}{\theta_{\Sigma}} \quad , \tag{50}$$

and

$$U_{\parallel} = \omega d \frac{\phi_T}{\phi_\Sigma} \cdot \frac{\theta_\Sigma}{\theta_T} . \tag{51}$$

Next, the introduction of the hub correction factors $(\sigma_{true}/\sigma)$ and $(U_{\parallel\, true}/U_{\parallel})$ results in the following expressions for the corrected values of conductivity and velocity.

$$\sigma_{corr} = \frac{2}{\mu \omega d^2} \frac{\phi_\Sigma}{\phi_{\Sigma\, cal}} \cdot \frac{(\sigma_{true}/\sigma)}{\theta_\Sigma} , \tag{52}$$

and

$$U_{\parallel\, corr} = \omega d \frac{\phi_T}{\phi_\Sigma} \frac{\theta_\Sigma}{\theta_T} (U_{\parallel\, true}/U_{\parallel}). \tag{53}$$

For sake of convenience and simplicity, the conductivity and velocity calibration constants, $C_\Sigma$ and $C_T$ respectively, are defined below.

$$C_\Sigma = \frac{2\,(\sigma_{true}/\sigma)}{\mu \omega d^2 \phi_{\Sigma\, cal}} \tag{54}$$

$$C_T = \omega d\,(U_{\parallel true}/\,U_{\parallel}) \tag{55}$$

The desired calibration equations now appear in a very simple form as

$$\sigma_{corr} = C_{\Sigma}\phi_{\Sigma} / \theta_{\Sigma} \tag{56}$$

and

$$U_{\parallel corr} = C_{T} \frac{\phi_{T}}{\phi_{\Sigma}} \cdot \frac{\theta_{\Sigma}}{\theta_{T}} \tag{57}$$

The calibration constants, $C_{\Sigma}$ and $C_{T}$ are determined by Figure 6.

Finally, the working of the probe is briefly summarized below.

1. Record calibration potential, $\phi_{\Sigma\, cal}$, with probe in room air.

2. Null both outputs of the probe.

3. Immerse the probe in the moving conducting medium and record $\phi_{\Sigma}$ and $\phi_{T}$.

4. With the help of Figure 6, calculate $C_{\Sigma}$ and $C_{T}$.

5. Equations (56) and (57) now furnish the corrected values of electrical conductivity, $\sigma_{corr}$, and stream velocity, $U_{\parallel\, corr}$.

# CHAPTER IV

# COMPARISON OF THEORETICAL AND EXPERIMENTAL RESULTS

This chapter begins with a discussion of experimental verification of the calibration method developed in the last section of Chapter III. Next, analytical values of the conductivity boundary correction factor, $\theta_{\Sigma}$, are compared with the experimental values. The concluding section includes a discussion of the experimental verification of the theoretical values of the conductivity hub correction factor, $\sigma_{true}/\sigma$ which, as previously mentioned, accounts for the finite size of the instrument.

The calibration equation for electrical conductivity, $\sigma$, Equation (52) reads

$$\sigma_{corr} = \frac{2}{\mu \omega d^2} \cdot \frac{\phi_{\Sigma}}{\phi_{\Sigma\, cal}} \cdot \frac{(\sigma_{true}/\sigma)}{\theta_{\Sigma}} \tag{52}$$

where the calibration potential, $\phi_{\Sigma\, cal}$, is given by Equation (45). If the probe were immersed in an unbounded medium of uniform conductivity, then Equation (52) simplifies to

$$\sigma_{corr} = \frac{2}{\mu \omega d^2} \cdot \frac{\phi_{\Sigma\infty}}{\phi_{\Sigma\, cal}} \cdot (\sigma_{true}/\sigma) \tag{58}$$

because, for an unbounded medium, the conductivity boundary correction factor, $\theta_{\Sigma}$, approaches unity (see, for example, Figures 3 and 4).

Four probes labeled A, B, C, and D were constructed and tested in cylindrical plexiglas containers filled with a saturated salt solution. The characteristics of the probes are tabulated below in Table 3. The electrical conductivity of the electrolyte, measured by a conductivity cell meter, was found to be 22.8 mhos/meter at room temperature of 23° C. The magnetic permeability, $\mu$, of the salt solution is the same as the magnetic permeability of free space $\mu_0$, and equals $1.257 \times 10^{-6}$ henrys/meter. A 100 $kH_z$, 1 watt, oscillating power was supplied to the primary coil. The calibration potential, $\phi_{\Sigma\,cal}$, was measured by the probe in room air.

Table 3. Characteristics of the probes tested

| Characteristic | Probe | | | |
|---|---|---|---|---|
| | A | B | C | D |
| Heat shield diameter, $2\rho_0$, cm | 1.03 | 1.03 | 1.03 | 0.42 |
| Coil spacing, d, cm | 1.91 | 2.54 | 3.18 | 1.14 |
| $2\rho_0/d$ | .542 | .407 | .325 | .365 |
| Hub correction factor, $\sigma_{true}/\sigma$ | 1.082[a] | 1.047 | 1.029 | 1.037 |
| Calibration potential, $\phi_{\Sigma\,cal}$, mv | 192.0 | 108.0 | 18.0 | 22.5 |

[a]Extrapolated value from Figure 6.

The perturbation potential-sum, $\phi_{\Sigma\infty}$ which would be induced in an unbounded medium was determined using an indirect approach. Each of the probes was immersed in the center of several deep plexiglas cylindrical containers of varying diameters filled with saturated salt solution of known electrical conductivity. The corresponding scope readings, $\phi_{\Sigma}$, were plotted against the reciprocal of container diameter, $(2R)^{-1}$. Two of the plots are shown in Figures 7 and 8. The plots were found to be linear and were extrapolated to $(2R)^{-1} = 0$ to obtain the value of $\phi_{\Sigma\infty}$, the output potential-sum of the probe in an unbounded medium. The values of the conductivity hub correction factors, $\sigma_{true}/\sigma$, were read from Figure 6. Then, the experimental values of electrical conductivity, $\sigma$, corrected for the presence of both the cylindrical boundary and the finite size probe, were computed using Equation (58). These values are compared with the conductivity cell measurements in Table 4. Note that in the case of probe D, a concentrated sulfuric acid solution was used in place of the salt solution because the data obtained with the latter could not be conveniently extrapolated.

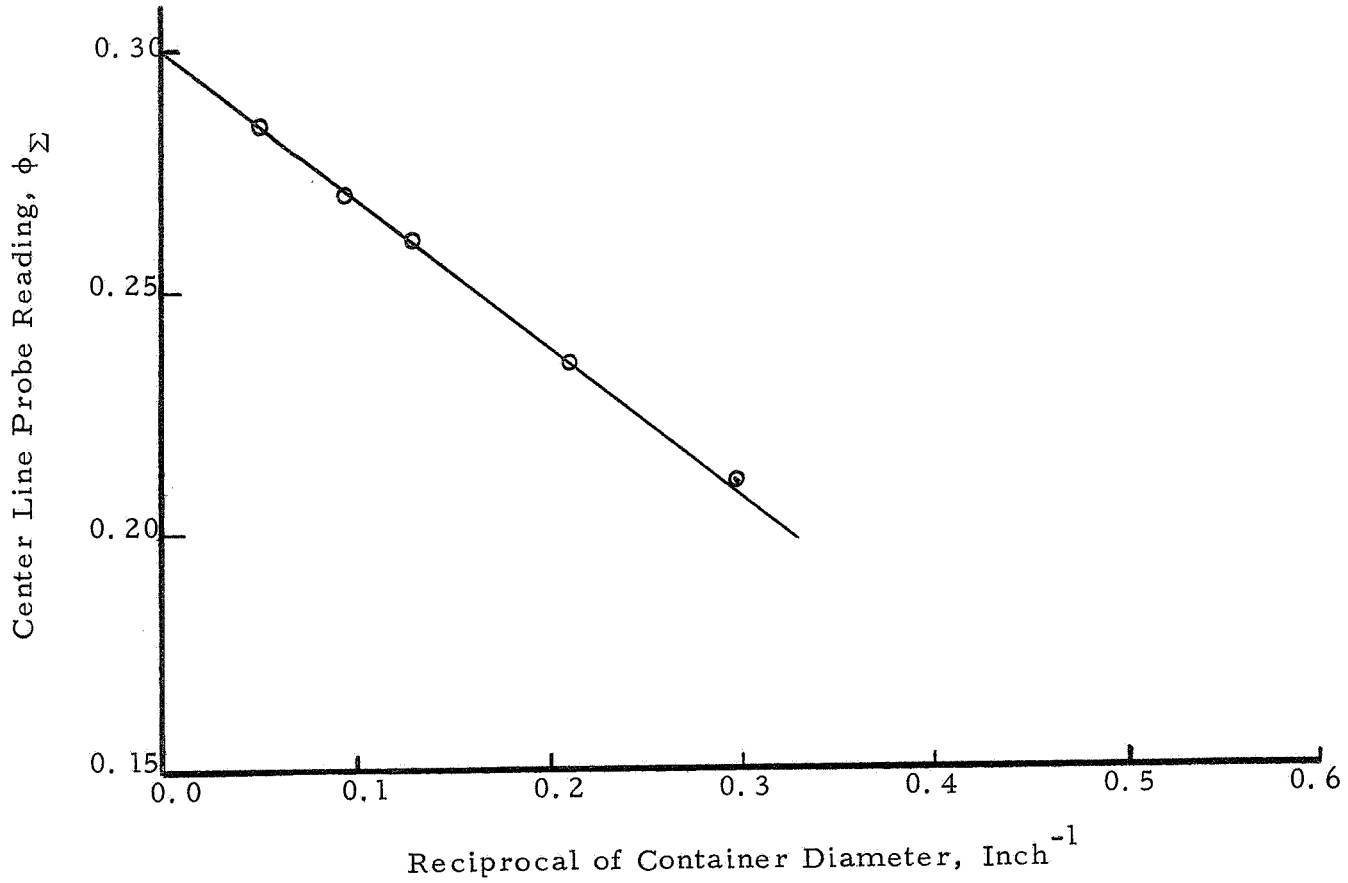


Figure 7. Center line probe reading $\phi_\Sigma$ as a function of reciprocal of container diameter $(2R)^{-1}$ for Probe C.

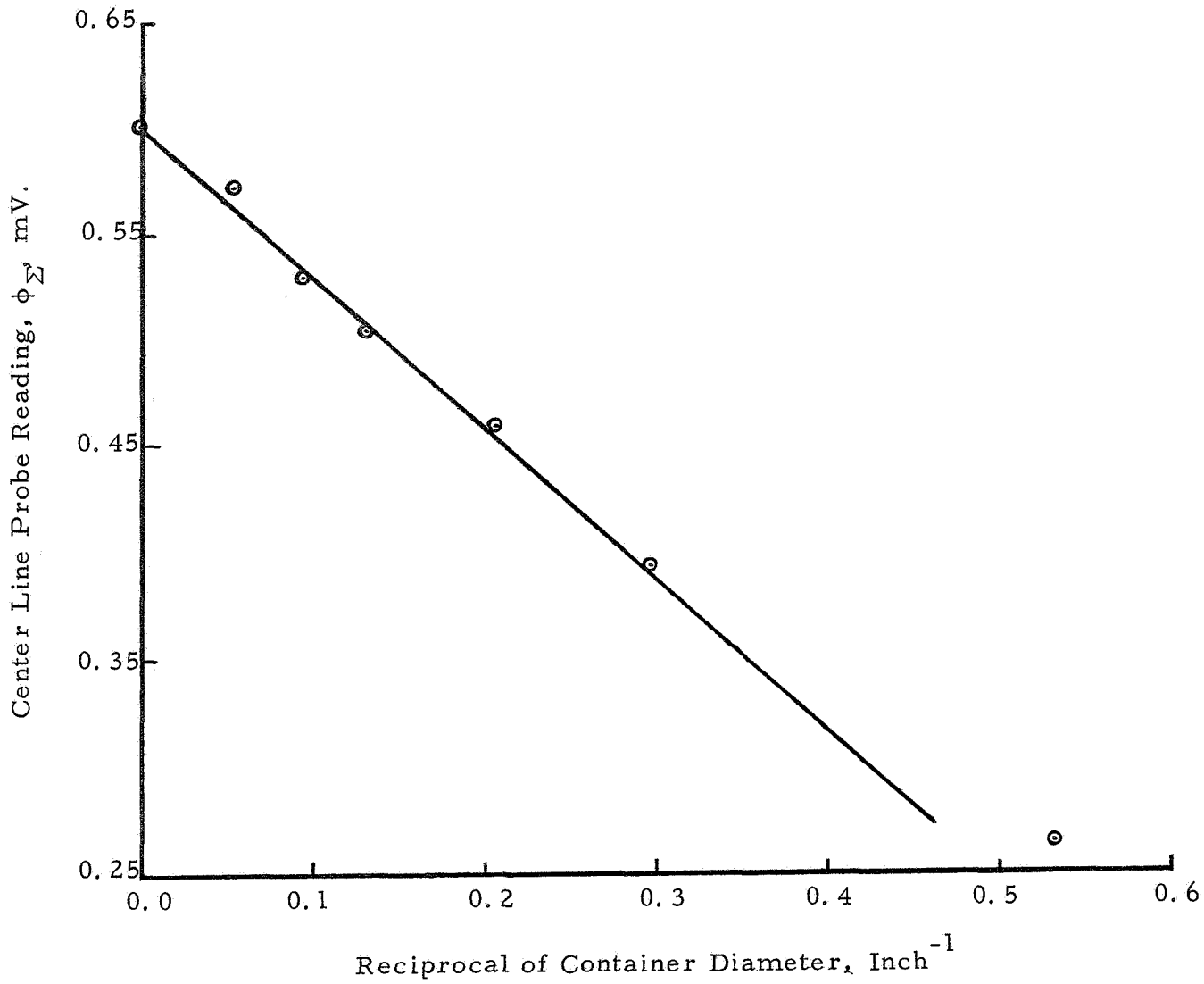


Figure 8. Center line probe reading $\phi_\Sigma$ as a function of reciprocal of container diameter $(2R)^{-1}$ for Probe B.

Table 4. Values of electrical conductivity using calibration equation and conductivity cell

| Probe label | $\sigma$ (Calibration Equation) mhos/meter | $\sigma$ (Cell Measurement) mhos/meter | % Difference |
|---|---|---|---|
| A | 21.7 | 22.7[a] | 4.40 |
| B | 20.8 | 22.7[a] | 8.50 |
| C | 22.6 | 22.7[a] | 0.44 |
| D | 71.8 | 71.5[b] | 0.42 |

[a] Saturated salt solution.
[b] Concentrated sulfuric acid solution.

It may be noted from Table 4 that the experimental values of the electrical conductivity, $\sigma$, computed with the help of the conductivity calibration equation are within 5 percent of the conductivity cell measurement for three of the probes, while the fourth probe agreed within 10 percent. These results confirm the validity of the conductivity calibration equation, Equation (52), as well as the theoretical analysis of Rossow and Posch (1966).

The analytical values of the conductivity correction factor, $\theta_{\Sigma}$, were experimentally verified using the probes A, B, and C. Two deep plexiglas cylindrical containers of different diameters were filled with a saturated salt solution having a conductivity of 22.8 mhos/meter. The perturbation potential-sum $\phi_{\Sigma}$, was recorded for

several different radial positions of the probes in each of the two cylinders. For each of the probes, these values of $\phi_\Sigma$ were divided by the experimentally determined value of $\phi_{\Sigma\infty}$ to obtain the values of $\theta_\Sigma$. Figure 9 illustrates a comparison of the analytical and experimental values of $\theta_\Sigma$ for two different values of the coil spacing parameter $D = d/R$. The analytical values were obtained, by interpolation, from Figure 3. The difference between analytical and experimental values is less than 5 percent except near the edge of the cylindrical boundary where the probe output was found to be extremely sensitive to the alinement of the probe's axis parallel to the axis of the cylindrical boundary. A comparison of experimental and analytical values of $\theta_\Sigma$ for the case $P = \rho/R = 0.0$ is presented in Figure 10. The deviation of the experimental data from the analytical results is well within 5 percent except when the coil spacing parameter, $D = d/R$, exceeds 0.6.

The analytical values of the conductivity hub correction factor, $\sigma_{true}/\sigma$, were experimentally verified as follows. A large cylindrical container of 19-inch diameter was filled with the saturated salt solution. Because the dimensions of the probes used were small as compared to the cylinder radius, therefore the solution in the container simulated an unbounded medium. The value of the perturbation potential-sum $\phi_{\Sigma\infty}$, was recorded with the probe immersed in the center of the

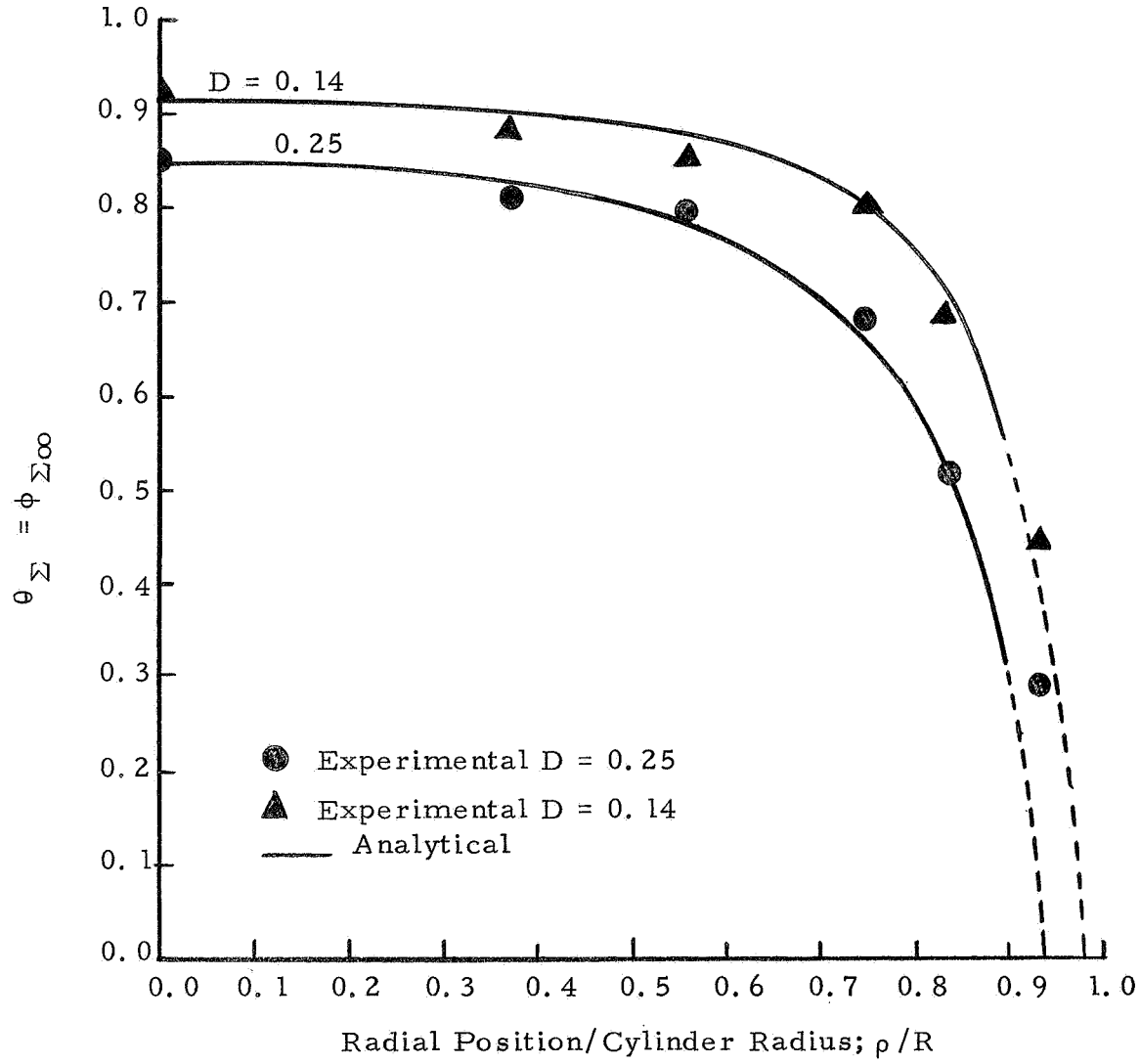


Figure 9. Comparison of numerical calculations of $\theta_\Sigma$ with experimental data taken by a coaxial probe in cylinders of salt solution.

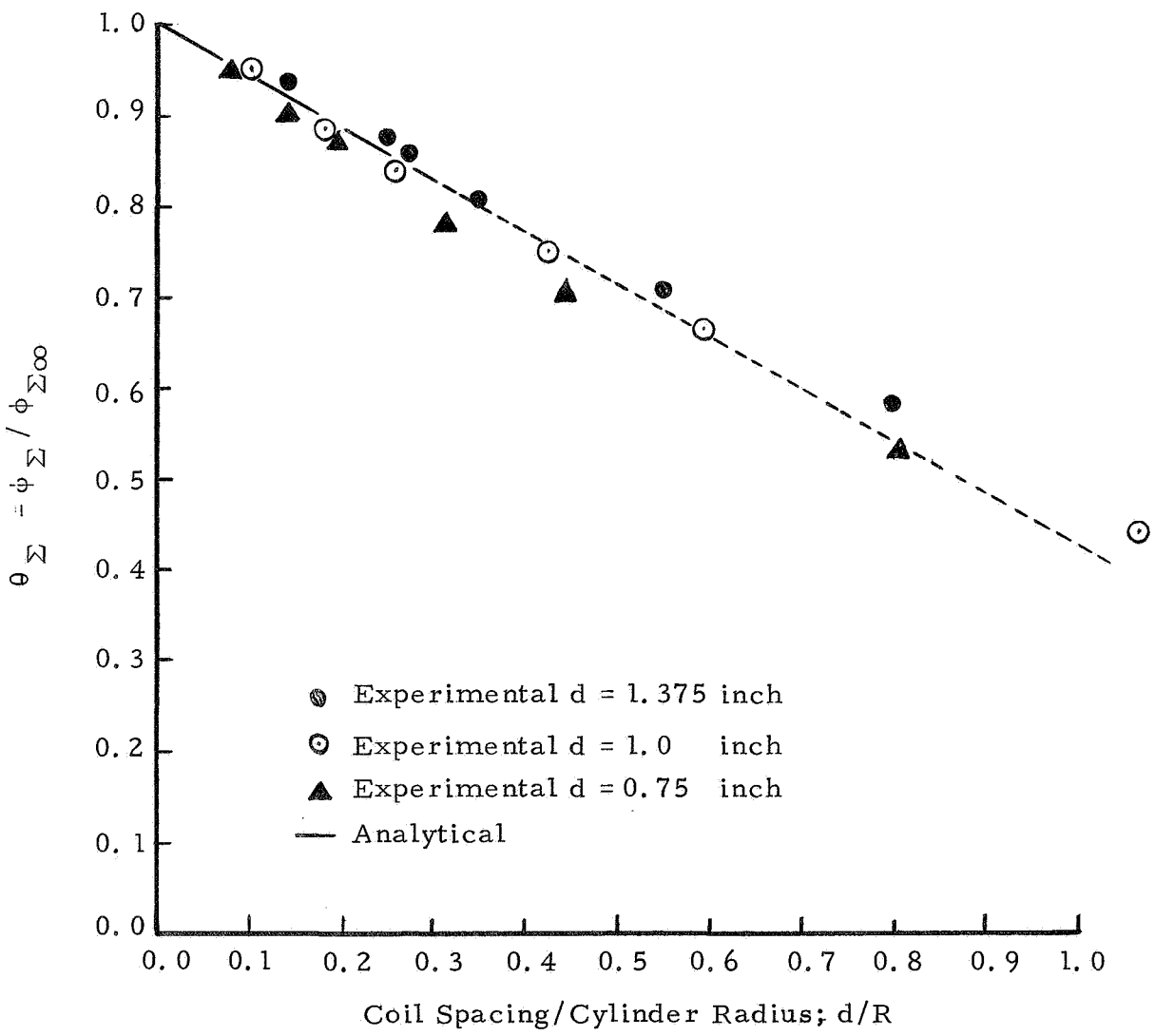


Figure 10. Comparison of numerical calculations of $\theta_\Sigma$ with experimental data taken by a coaxial probe in cylinders of slat solution for the case of $P = \rho/R = 0.0$.

cylinder. With calibration potential, $\phi_{\Sigma\,cal}$, obtained as discussed earlier and hub correction factor, $\sigma_{true}/\sigma$ read from Figure 6, the value of electrical conductivity, corrected for finite probe size, was calculated with the help of Equation (58). The procedure was repeated for three different diameters of the quartz tubing. The values of conductivity, so obtained, were then compared with the conductivity cell measurements. A sample of the data taken with probe C is presented in a tabular form in Table 5 below, and it can be seen that the comparison is favorable, the maximum difference being less than 6 percent. Thus, the validity of the conductivity hub correction factors is confirmed.

Table 5. Experimental verification of the theoretical values of the conductivity hub correction factors

| Quartz tubing diameter, $2\rho_0$, cm | $2\rho_0/d$ | Probe output, $\phi_{\Sigma\infty}$, mv | $\frac{\sigma_{true}}{\sigma}$ | Conductivity, $\sigma$, mhos/meter | Conductivity cell measurement, mhos/meter | % difference |
|---|---|---|---|---|---|---|
| 1.0 | 0.325 | 1.225 | 1.029 | 21.7 | 22.7 | 4.40 |
| 1.5 | 0.475 | 1.175 | 1.064 | 21.6 | 22.7 | 4.85 |
| 2.0 | 0.650 | 1.050 | 1.118[a] | 21.4 | 22.7 | 5.70 |

[a]Extrapolated from Figure 6.

# CHAPTER V

## CONCLUDING REMARKS

Tests conducted in cylindrical containers filled with saturated salt solution furnished reasonable experimental confirmation of the analytical values of the conductivity correction factor for a cylindrical boundary, $\theta_{\Sigma}$, for several different values of the coil spacing parameter, $D = d/R$, and the radial position parameter $P = \rho/R$. The tests also established the validity of the analytical values of the conductivity hub correction factor, $\sigma_{true}/\sigma$, for three different values of the dimensionless parameter $2\ \rho_0/d$.

However, outside of the plasma wind-tunnel, experimental verification of the theoretical values of the velocity cylindrical boundary correction factor, $\theta_{\mathbb{T}}$, and velocity hub correction factor, $U_{\parallel\ true}/U_{\parallel}$ was not attempted because of practical difficulties in attaining such values of $\sigma\ U_{\parallel}$ as would be large enough to give rise to probe outputs which can be conveniently measured.

Experiments have recently been concluded at Ames Research Center, Moffett Field, California by Vendell and Posch which reveal a 10 percent agreement between the center line velocity measurements in a constricted-arc wind-tunnel made by the coaxial probe and by other independent techniques such as a spark-injection method used by

Jedlicka (1968) and the sharp-edged flow-swallowing enthalpy probes of Anderson and Sheldahl (1968). However, the center line conductivity measurements made by the coaxial probe could not be verified because no other measurements of the local conductivity of this plasma facility by independent techniques have been made.

Finally, the electrical time response and the low thermal sensitivity of the coaxial instrument were found to be significantly improved as compared with the three-sting probe.

Although the favorable agreement of the analytical and experimental results justifies the theory of the probe, some additional development is needed. In particular, the following aspects warrant further attention.

1. An oscillator having several output frequencies should be used with the probe to investigate the effect of the impressed frequency, $\omega/2\pi$, upon the performance of the probe.

2. If possible, it would be desirable to decrease the electrical time response and increase the thermal time response of the probe.

3. Although the results obtained with the coaxial probe in a low-density plasma stream were satisfactory, the three-coil instrument should be tested in higher density plasmas.

# LITERATURE CITED

Akimov, A. V. and O. R. Koneko. 1966. Measurement of Plasma Conductivity by a Radio-Frequency Method. Soviet Phys.-Tech. Phys. 10:1126-1127

Anderson, L. A. and R. E. Sheldahl. 1968. Flow-Swallowing Enthalpy Probes in Low-Density Plasma Streams. AIAA Paper Number 68-390.

Barkan, P. and A. M. Whitman. 1966. A Means for the Study of the Stagnation Pressure Distribution in a Current-Carrying Plasma. AIAA Preprint:66-179.

Blackman, V. H. 1959. Magnetohydrodynamic Flow Experiment of a Steady State Nature. ARS Preprint:1007-59.

Carter, A. F., D. R. McFarland, W. R. Weaver, S. K. Park, and G. P. Wood. 1966. Operating Characteristics, Velocity and Pitot Distribution and Material Evaluation Tests in the Langley One-In.-Square Plasma Acclerator. AIAA Preprint:66-180.

Donskoi, K. V., Y. A. Dunaev, and I. A. Prokof'ev. 1963. Measurement of Electrical Conductivity in Gas Streams. Soviet Phys.-Tech. Phys. 7:805-807.

Fuhs, A. E. 1964. An Instrument to Measure Velocity-Electrical Conductivity of Arc Plasmajets. AIAA Journal 2:667-673.

Jedlicka, J. R. 1968. Private Communications. Ames Research Center, Moffett Field, California.

Koritz, H. E. and J. C. Keck. 1964. Technique for Measuring the Electrical Conductivity of Wakes of Projectiles at Hypersonic Speeds. Review of Scientific Instruments 35 (2):201-208.

Lin, S. C., E. L. Resler, and A. Kantrowitz. 1955. Electrical Conductivity of Highly Ionized Argon Gases Produced by Shock Waves. Journal of Applied Physics 26 (1):95-109.

Luther, A. H. 1963. A Non-Uniform-Plasma, Electrical Conductivity Probe. U. S. Naval Ordnance Laboratory TR 63-165.

Olson, R. A. and E. C. Lary. 1962. Electrodeless Plasma Conductivity Probe Apparatus. Review of Scientific Instruments 33 (12): 1350-1353.

Persson, K. B. 1961. A Method for Measuring the Conductivity in a High Electron Density Plasma. Journal of Applied Physics 32 (12): 2631-2640.

Poberezhskii, L. P. 1964. Measurement of Velocity and Electrical Conductivity of an Ionized Gas Stream. Soviet Phys.-Tech. Phys. 8:1088-1092.

Rossow, V. J. 1959. On Series Expansions in Magnetic Reynolds Number. NASA TN D-10.

Rossow, V. J. and R. E. Posch. 1966. Coil Systems for Measuring Conductivity and Velocity of Plasma Streams. Review of Scientific Instruments 37 (9):1232-1242.

Savic, P. and G. T. Boult. 1962. A Frequency Modulation Circuit for the Measurement of Gas Conductivity and Boundary Layer Thickness in a Shock Tube. Journal of Scientific Instruments 39:258-266.

Stine, H. A., V. R. Watson, and C. E. Shepard. 1964. Effect of Axial Flow on the Behavior of the Wall-Constricted Arc. NASA TM X-54, 065.

Stratton, J. A. 1941. Electromagnetic Theory. McGraw-Hill, New York, New York.

Stubbe, E. J. 1966. A Measurement of the Electrical Conductivity of Plasmas. AIAA Preprint:66-181. Plasmadynamics Conference, Monterey, California.

Tanaka, H. and M. Hagi. 1964. A Method of Measurement of Plasma Conductivity. II. Example of Measurement. Japanese Journal of Applied Physics 3:338-341.

Vendell, E. W. 1967. Boundary Corrections for a Three-Coil Condictivity/Velocity Plasma Probe. Ph. D. dissertation, Oklahoma State University, Stillwater, Oklahoma.

Vendell, E. W. 1968. Boundary Corrections for a Three-Coil Conductivity/Velocity Plasma Probe. NASA Technical Note D-4538.

# VITA

Vikram Kumar Kinra

Candidate for the Degree of

Master of Science

Thesis: Boundary Corrections for a Coaxial Three-Coil Conductivity/ Velocity Plasma Probe

Major Field: Mechanical Engineering

Biographical Information:

Personal Data: Born at Lyallpur, India, April 3, 1946, son of Gurmukh Chand and Gian Vati Kinra; single.

Education: Attended high school in Rohtak, Hariana, India; received the Bachelor of Technology degree from Indian Institute of Technology, Kanpur, majoring in Mechanical Engineering, 1967; completed requirements for the Master of Science degree in Mechanical Engineering at Utah State University in 1968.